

# Temporal Spike Sequence Learning via Backpropagation for Deep Spiking Neural Networks

Wenrui Zhang<sup>1</sup> Peng Li<sup>1</sup>

## Abstract

Spiking neural networks (SNNs) are well suited for spatio-temporal learning and implementations on energy-efficient event-driven neuromorphic processors. However, existing SNNs error backpropagation (BP) track methods lack proper handling of spiking discontinuities and suffer from low performance compared to BP methods for traditional artificial neural networks. In addition, a large number of time steps are typically required for SNNs to achieve decent performance, leading to high latency and rendering spike based computation unscalable to deep architectures. We present a novel Temporal Spike Sequence Learning Backpropagation (TSSL-BP) method for training deep SNNs, which breaks down error backpropagation across two types of inter-neuron and intra-neuron dependencies. It considers the all-or-none characteristics of firing activities, capturing inter-neuron dependencies through presynaptic firing times, and internal evolution of each neuronal state through time capturing intra-neuron dependencies. For various image classification datasets, TSSL-BP efficiently trains deep SNNs within a short temporal time window of a few steps with improved accuracy and runtime efficiency including achieving more than 2% accuracy improvement over the previously reported SNN work on CIFAR10.

## 1. Introduction

Spiking neural networks (SNNs), a brain-inspired computational model, have gathered significant research interests during recent years. Unlike neurons in artificial neural networks (ANNs) that are characterized by a single, static, and continuous-valued activation function, SNNs compute based upon discrete spike events and spatio-temporal patterns (Ger-

stner & Kistler, 2002). The spike-based operational principles of SNNs have rendered energy-efficient VLSI neuromorphic chips such as IBM’s TrueNorth (Akopyan et al., 2015) and Intel’s Loihi (Davies et al., 2018). Despite the recent progress in SNNs and neuromorphic processor designs, fully leveraging the theoretical computing advantages of SNNs over traditional artificial neural networks (ANNs) (Maass et al., 2002) to achieve a greater computational performance remains challenging.

Inspired by the success of error backpropagation (BP) and its variants in training conventional deep neural networks (DNNs), various SNNs BP methods have emerged, aiming at attaining the same level of performance (Bohte et al., 2002; Lee et al., 2016; Wu et al., 2018; Jin et al., 2018; Shrestha & Orchard, 2018; Zhang & Li, 2019). Although many appealing results are achieved by these methods, developing SNNs BP training methods that are a par with the mature BP tools widely available for training ANNs today is a nontrivial problem (Tavanaei et al., 2018).

Training of SNNs via BP are challenged by two fundamental issues. First, from an algorithmic perspective, the complex neural dynamics in both spatial and temporal domains make the BP process obscure. Moreover, the errors are hard to be precisely backpropagated due to the non-differentiability of discrete spike events. Second, a large number of time steps are typically required for emulating SNNs in time to achieve decent performance, leading to high latency and rendering spike based computation unscalable to deep architectures. It is desirable to demonstrate the success of BP in training deeper SNNs achieving satisfactory performances on more challenging datasets.

In this paper, we demonstrate a powerful new SNNs BP method, called temporal spike sequence learning via BP (TSSL-BP), to learn any target output temporal spiking sequences. TSSL-BP acts as a universal training method for any employed spike codes (rate, temporal, and combinations of thereof). To tackle the aforementioned difficulties, TSSL-BP breaks down error backpropagation across two types of inter-neuron and intra-neuron dependencies. It considers the all-or-none characteristics of firing activities, capturing inter-neuron dependencies through presynaptic firing times. And it considers internal evolution of each neuronal state

<sup>1</sup>Department of Electrical and Computer Engineering, University of California, Santa Barbara, Santa Barbara, CA 93106. Correspondence to: Peng Li <lip@ucsb.edu>.

through time, capturing intra-neuron dependencies. The effectiveness and precision of TSSL-BP makes it possible to successfully train SNNs over a very short temporal window, e.g. over 5-10 time steps, enabling ultra-low latency spike computation. As demonstrated in Section 4, TSSL-BP significantly improves accuracy and runtime efficiency of BP training on several well-known image datasets of MNIST (LeCun et al., 1998), FashionMNIST (Xiao et al., 2017), and CIFAR10 (Krizhevsky et al., 2014). Specifically, it achieves more than 2% accuracy improvement over the previously reported SNN work on CIFAR10, a challenging dataset for all prior SNNs BP methods.

## 2. Background

### 2.1. Existing Backpropagation methods for SNNs

One of the earliest SNNs BP methods is the well-known SpikeProp algorithm (Bohte et al., 2002). However, it is restricted to SNNs in which each neuron only spikes once. SpikeProp has been extended for more general cases (Booij & Nguyen, 2005; Ghosh-Dastidar & Adeli, 2009; Xu et al., 2013) which are still limited to single spike per output neuron without demonstrating success on real-world tasks.

On the other hand, it is popular to train an ANN and then approximately convert it to an SNN (Diehl et al., 2015; Esser et al., 2015; Hunsberger & Eliasmith, 2016; Sengupta et al., 2019). Nevertheless, such conversion leads to approximation errors and gives up the opportunity in exploiting SNNs' temporal learning capability.

Recently, training SNNs with BP under a firing rate (or activity level) coded loss function has been shown to deliver competitive performances (Lee et al., 2016; Wu et al., 2018; Shrestha & Orchard, 2018; Jin et al., 2018; Zhang & Li, 2019). Among them, (Lee et al., 2016) does not consider the temporal correlations of neural activities and treats spiking times as noise to allow error gradient computation.

(Wu et al., 2018) and (Shrestha & Orchard, 2018) capture the temporal effects by performing backpropagation through time (BPTT) (Werbos, 1990). However, (Shrestha & Orchard, 2018) gets around the non-differentiability of spike events by approximating the spiking process via a probability density function of spike state change. Similarly, (Wu et al., 2018) computes the error gradient based on the continuous membrane waveforms resulted from smoothing out all spikes. These approximations treat the spiking neurons' activation as a differentiable signal analogous to the activation functions in ANNs, leading to inconsistency between the computed gradient and target loss, and thus degrade training performance.

(Jin et al., 2018; Zhang & Li, 2019) present spike-train level BP methods for training deep SNNs. These methods can

more accurately capture the effects of the non-differentiable activation function of spiking neurons aggregated at the spike train level without resorting to various microscopic approximation errors of the previous approaches. However, the length of spike trains over which BP is applied needs to be long enough to achieve decent performance, leading to long inference latency and high training cost.

(Wu et al., 2019) extends the method in (Wu et al., 2018) by adding optimization techniques such as neuron normalization and population decoding. It can train SNNs to achieve encouraging performances over a relatively small number of time steps. Since at its core lies the method of (Wu et al., 2018), it still approximates the all-or-none firing characteristics of spiking neurons by a continuous activation function, causing the same problems introduced before.

In this work, we propose the TSSL-BP method as a universal training method for any employed spike codes. It can not only precisely capture the temporal dependencies but also allow ultra-low latency inference and training over only five time steps while achieving excellent accuracies.

### 2.2. Spiking Neuron Model

SNNs employ a more biologically plausible spiking neuron model than ANNs. We introduce the leaky integrate-and-fire (LIF) neuron model and synaptic model (Gerstner & Kistler, 2002) adopted in this work.

Consider the input spike train from pre-synaptic neuron  $j$  to neuron  $i$ :  $s_j(t) = \sum_{t_j^{(f)}} \delta(t - t_j^{(f)})$ , where  $t_j^{(f)}$  denotes a particular firing time of presynaptic neuron  $j$ . The incoming spikes are converted into an (unweighted) postsynaptic potential (PSC)  $a_j(t)$  through a synaptic model. The neuronal membrane voltage  $u_i(t)$  at time  $t$  for neuron  $i$  is given by

$$\tau_m \frac{du_i(t)}{dt} = -u_i(t) + R \sum_j w_{ij} a_j(t) + \eta_i(t), \quad (1)$$

where  $R$  and  $\tau_m$  are the effective leaky resistance and time constant of the membrane,  $w_{ij}$  is the synaptic weight from pre-synaptic neuron  $j$  to neuron  $i$ ,  $a_j(t)$  is the (unweighted) postsynaptic potential (PSC) induced by the spikes from pre-synaptic neuron  $j$ , and  $\eta(t)$  denotes the reset function.

The PSC and the reset function can be written as

$$a_j(t) = (\epsilon * s_j)(t) \quad \eta_i(t) = (\nu * s_i)(t), \quad (2)$$

where  $\epsilon(\cdot)$  and  $\nu(\cdot)$  are the spike response and reset kernel, respectively. The reset kernel reduces the membrane potential by a certain amount  $\Delta_R$ , where  $\Delta_R$  is equal to the firing threshold right after the neuron fires and then decays over time according to the time constant of the membrane potential  $\tau_m$ . In this work, we adopt a first order synaptic model as the spike response kernel.

Considering the discrete time steps simulation, we use the fixed-step first-order Euler method to discretize (1) to

$$u_i[t] = \theta_\tau u_i[t-1] + \sum_j w_{ij} a_j[t] + \eta_i[t], \quad (3)$$

where  $\theta_\tau = 1 - \frac{1}{\tau_m}$  denotes the dependency of the membrane voltage  $u_i[t]$  on its value  $u_i[t-1]$  at the previous time point. The ratio of R and  $\tau_m$  is absorbed into the synaptic weight. The reset function  $\eta_i[t]$  represents the firing-and-resetting mechanism of the neuron model. Moreover, the firing output of the neuron is expressed as

$$s_i[t] = H(u_i[t] - V_{th}), \quad (4)$$

where  $V_{th}$  is the firing threshold and  $H(\cdot)$  is the Heaviside step function.

### 3. Methods

#### 3.1. Forward Pass

Without loss of generality, we consider performing BP across two adjacent layers  $l-1$  and  $l$  with  $N_{l-1}$  and  $N_l$  neurons, respectively, in a fully-connected feedforward SNNs as shown in Figure 1. The procedure can be also applied to convolutional and pooling layers. Denote the presynaptic weights by  $\mathbf{W}^{(l)} = [\mathbf{w}_1^{(l)}, \dots, \mathbf{w}_{N_l}^{(l)}]^T$ , PSCs from neurons in layer  $l-1$  by  $\mathbf{a}^{(l-1)}[t] = [a_1^{(l-1)}[t], \dots, a_{N_{l-1}}^{(l-1)}[t]]$ , spike trains output of the  $l-1$  layer by  $\mathbf{s}^{(l-1)}[t] = [s_1^{(l-1)}[t], \dots, s_{N_{l-1}}^{(l-1)}[t]]$ , membrane potentials and the corresponding output spike trains of the  $l$  layer neurons respectively by  $\mathbf{u}^{(l)}[t] = [u_1^{(l)}[t], \dots, u_{N_l}^{(l)}[t]]$  and  $\mathbf{s}^{(l)}[t] = [s_1^{(l)}[t], \dots, s_{N_l}^{(l)}[t]]$ , where variables associated with neurons in the layer  $l$  have  $l$  as the superscript.

The forward propagation between the two layers is described as

$$\begin{aligned} \mathbf{a}^{(l-1)}[t] &= (\epsilon * \mathbf{s}^{(l-1)}[t]) \\ \mathbf{u}^{(l)}[t] &= \theta_\tau \mathbf{u}^{(l)}[t-1] + \mathbf{W}^{(l)} \mathbf{a}^{(l-1)}[t] + (\nu * \mathbf{s}^{(l)}[t]) \\ \mathbf{s}^{(l)}[t] &= H(\mathbf{u}^{(l)}[t] - V_{th}) \end{aligned} \quad (5)$$

In the forward pass, the spike trains  $\mathbf{s}^{(l-1)}[t]$  of the  $l-1$  layer generate the (unweighted) PSCs  $\mathbf{a}^{(l-1)}[t]$  according to the synaptic model. Then,  $\mathbf{a}^{(l-1)}[t]$  are multiplied the synaptic weights and passed onto the neurons of layer  $l$ . The integrated PSCs alter the membrane potentials and trigger the output spikes of the layer  $l$  neurons when the membrane potentials exceed the threshold.

#### 3.2. The Loss Function

The goal of the proposed TSSL-BP method is to train a given SNN in such a way that each output neuron learns

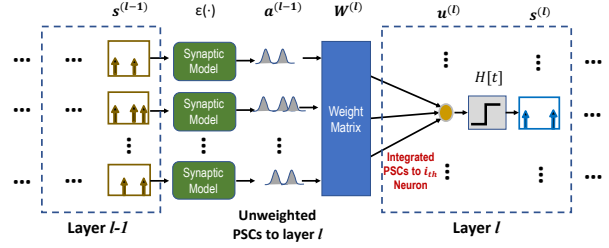


Figure 1. Forward evaluation pass of SNNs.

to produce an desired firing sequence arbitrarily specified by the user according to the input class label. Denote the desired and the actual spike trains in the output layer by  $\mathbf{d} = [\mathbf{d}[t_0], \dots, \mathbf{d}[t_{N_t}]]$  and  $\mathbf{s} = [\mathbf{s}[t_0], \dots, \mathbf{s}[t_{N_t}]]$  where  $N_t$  is the number of the considered time steps,  $\mathbf{d}[t]$  and  $\mathbf{s}[t]$  the desired and actual firing events for all output neurons at time  $t$ , respectively.

The loss function  $L$  can be defined using any suitable distance function measuring the difference between  $\mathbf{d}$  and  $\mathbf{s}$ . For example, using the mean square error for each output neuron at each time step defines the following loss

$$\begin{aligned} L &= \sum_{k=0}^{N_t} E[t_k] = \frac{1}{2} \sum_{k=0}^{N_t} (\mathbf{d}[t_k] - \mathbf{s}[t_k])^2 \\ &= \frac{1}{2} \sum_i \|\mathbf{d} - \mathbf{s}\|_2^2, \end{aligned} \quad (6)$$

where  $E[t]$  is the error at time  $t$ . The loss can be also defined by using a kernel function (Shrestha & Orchard, 2018). Using the spike response kernel  $\epsilon(\cdot)$ , one defines the error at each time step as

$$E[t] = (\epsilon * \mathbf{d})[t] - (\epsilon * \mathbf{s})[t] = \mathbf{a}_d[t] - \mathbf{a}_s[t]. \quad (7)$$

#### 3.3. Temporal Spike Sequence Learning via Backpropagation (TSSL-BP) Method

Without loss of generality, we adopt (7) to define the total loss

$$L = \sum_{k=0}^{N_t} E[t_k] = \frac{1}{2} \sum_{k=0}^{N_t} (\mathbf{a}_d[t_k] - \mathbf{a}_s[t_k])^2. \quad (8)$$

For the neurons in layer  $l$ , the error gradient with respect to the presynaptic weights matrix  $\mathbf{W}^{(l)}$  is

$$\frac{\partial L}{\partial \mathbf{W}^{(l)}} = \sum_{k=0}^{N_t} \frac{\partial E[t_k]}{\partial \mathbf{W}^{(l)}}. \quad (9)$$

(5) reveals that the values of  $\mathbf{u}^{(l)}$  at time  $t_k$  have contribution

to all future fires and losses. Using the chain rule, we get

$$\begin{aligned} \frac{\partial L}{\partial \mathbf{W}^{(l)}} &= \sum_{k=0}^{N_t} \sum_{m=0}^k \frac{\partial E[t_k]}{\partial \mathbf{u}^{(l)}[t_m]} \frac{\partial \mathbf{u}^{(l)}[t_m]}{\partial \mathbf{W}^{(l)}} \\ &= \sum_{m=0}^{N_t} \mathbf{a}^{(l-1)}[t_m] \sum_{k=m}^{N_t} \frac{\partial E[t_k]}{\partial \mathbf{u}^{(l)}[t_m]}. \end{aligned} \quad (10)$$

Similar to the conventional backpropagation, we use  $\delta$  to denote the back propagated error at time  $t_m$  as  $\delta^{(l)}[t_m] = \sum_{k=m}^{N_t} \frac{\partial E[t_k]}{\partial \mathbf{u}^{(l)}[t_m]}$ .

Therefore, the weights update formula (10) can be written as

$$\frac{\partial L}{\partial \mathbf{W}^{(l)}} = \sum_{m=0}^{N_t} \mathbf{a}^{(l-1)}[t_m] \delta^{(l)}[t_m]. \quad (11)$$

$\mathbf{a}^{(l-1)}[t_m]$  is analogous to the pre-activation in the traditional ANNs which can be easily obtained from (5).  $\delta^{(l)}[t_m]$  is considered in two cases.

[*l* is the output layer.] The  $\delta^{(l)}[t_m]$  can be computed from

$$\delta^{(l)}[t_m] = \sum_{k=m}^{N_t} \frac{\partial E[t_k]}{\partial \mathbf{a}^{(l)}[t_k]} \frac{\partial \mathbf{a}^{(l)}[t_k]}{\partial \mathbf{u}^{(l)}[t_m]}. \quad (12)$$

From (8), the first term of (12) is given by

$$\frac{\partial E[t_k]}{\partial \mathbf{a}^{(l)}[t_k]} = \frac{1}{2} \frac{\partial (\mathbf{a}_d[t_k] - \mathbf{a}^{(l)}[t_k])^2}{\partial \mathbf{a}^{(l)}[t_k]} = \mathbf{a}^{(l)}[t_k] - \mathbf{a}_d[t_k] \quad (13)$$

The second term  $\frac{\partial \mathbf{a}^{(l)}[t_k]}{\partial \mathbf{u}^{(l)}[t_m]}$  is the key part of the TSSL-BP method and is discussed in Section 3.3.3 and 3.3.4.

[*l* is a hidden layer.]  $\delta^{(l)}[t_m]$  is derived using the chain rule and (5).

$$\begin{aligned} \delta^{(l)}[t_m] &= \sum_{j=m}^{N_t} \sum_{k=m}^j \frac{\partial \mathbf{a}^{(l)}[t_k]}{\partial \mathbf{u}^{(l)}[t_m]} \left( \frac{\partial \mathbf{u}^{(l+1)}[t_k]}{\partial \mathbf{a}^{(l)}[t_k]} \frac{\partial E[t_j]}{\partial \mathbf{u}^{(l+1)}[t_k]} \right) \\ &= \sum_{k=m}^{N_t} \frac{\partial \mathbf{a}^{(l)}[t_k]}{\partial \mathbf{u}^{(l)}[t_m]} \sum_{j=k}^{N_t} \frac{\partial \mathbf{u}^{(l+1)}[t_k]}{\partial \mathbf{a}^{(l)}[t_k]} \frac{\partial E[t_j]}{\partial \mathbf{u}^{(l+1)}[t_k]} \\ &= \sum_{k=m}^{N_t} \frac{\partial \mathbf{a}^{(l)}[t_k]}{\partial \mathbf{u}^{(l)}[t_m]} (\mathbf{W}^{(l+1)})^T \delta^{(l+1)}[t_k] \end{aligned} \quad (14)$$

(14) maps the error  $\delta$  from layer  $l+1$  to layer  $l$ . It is obtained from the fact that membrane potentials  $\mathbf{u}^{(l)}$  of the neurons in layer  $l$  influence their (unweighted) corresponding postsynaptic currents (PSCs)  $\mathbf{a}^{(l)}$  through fired spikes, and  $\mathbf{a}^{(l)}$  further affect the neuronal membrane potentials  $\mathbf{u}^{(l+1)}$  in the next layer.

### 3.3.1. KEY CHALLENGES IN SNN BACKPROPAGATION

As shown above, for both the output layer and hidden layers, once  $\frac{\partial \mathbf{a}^{(l)}[t_k]}{\partial \mathbf{u}^{(l)}[t_m]} (t_k \geq t_m)$  are known, the error  $\delta$  can be back propagated and the gradient of each layer can be calculated.

Importantly, the dependencies of the postsynaptic currents on the corresponding membrane potentials of the same neurons reflected in  $\frac{\partial \mathbf{a}^{(l)}[t_k]}{\partial \mathbf{u}^{(l)}[t_m]} (t_k \geq t_m)$  are due to the following spiking neural behaviors: a change in the neuronal membrane potential may bring it up to the firing threshold, and hence activate the corresponding neuron by generating an output spike, which in turn produces a postsynaptic current. Computing  $\frac{\partial \mathbf{a}^{(l)}[t_k]}{\partial \mathbf{u}^{(l)}[t_m]} (t_k \geq t_m)$  involves the activation of each neuron, i.e. firing a spike due to the membrane potential's crossing the firing threshold from below. Unfortunately, the all-or-none firing characteristics of spiking neurons makes the activation function nondifferentiable, introducing several key challenges.

A typical strategy in dealing with the non-differentiability of the activation in various prior works is to smooth the activation function by approximating it using a differentiable curve (Wu et al., 2018) as shown in the Figure 2, or a continuous probability density function (Shrestha & Orchard, 2018), which is similar to the former approach in spirit. However, these approaches effectively spread each discrete firing spike continuously over time, converting one actual spike to multiple fictitious spikes and also generating multiple fictitious postsynaptic currents displaced at different time points. We stress that while smoothing circumvents the numerical challenges brought by non-differentiability of the spiking activation, it effectively alters the underlying spiking neuron model and firing times, and leads to degraded accuracy in the error gradient computation. It is important to reflect that spike timing is the hallmark of spiking neural computation, altering firing times in BP can hamper precise learning of the targeted firing sequences as pursued in this paper.

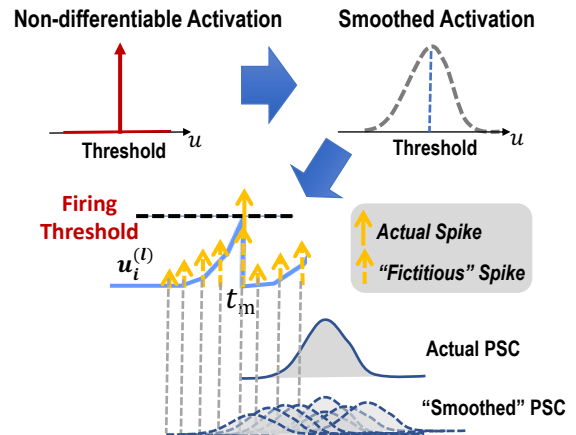


Figure 2. Fictitious smoothing of activation



### 3.3.2. THE MAIN IDEAS BEHIND TSSL-BP

The proposed TSSL-BP method aims to address the two key limitations of the prior BP methods: lack proper handling of spiking discontinuities and need for large numbers of time steps (i.e. high latency) for ensuring good performance. TSSL-BP computes  $\frac{\partial a_i^{(l)}[t_k]}{\partial u_i^{(l)}[t_m]}$  across two categories of spatio-temporal dependencies in the network: **inter-neuron** and **intra-neuron** dependencies. As shown in Figure 3, our key observations are: 1) temporal dependencies of a postsynaptic neuron on any of its presynaptic neurons *only* take place via the presynaptic spikes which generate PSCs to the postsynaptic neuron, and shall be considered as inter-neuron dependencies; 2) furthermore, each neuron’s state (i.e. membrane potential) evolves over time, introducing temporal dependencies of the state on its previous state values, which shall be captured as intra-neuron dependencies.

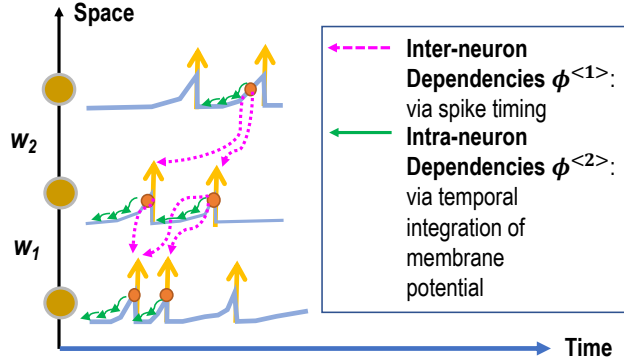


Figure 3. Inter-neuron and intra-neuron dependencies.

In the following, we show how to derive the required key derivative  $\frac{\partial a_i^{(l)}[t_k]}{\partial u_i^{(l)}[t_m]}$  ( $t_k \geq t_m$ ) for each neuron  $i$  in layer

$l$ . We denote  $\phi_i(t_k, t_m) = \frac{\partial a_i^{(l)}[t_k]}{\partial u_i^{(l)}[t_m]} = \phi_i^{<1>}(t_k, t_m) + \phi_i^{<2>}(t_k, t_m)$ , where  $\phi_i^{<1>}(t_k, t_m)$  represents the inter-neuron dependency and  $\phi_i^{<2>}(t_k, t_m)$  is the intra-neuron dependency.

### 3.3.3. INTER-NEURON BACKPROPAGATION

Instead of performing the problematic activation smoothing, we critically note that the all-or-none characteristics of firing behavior is such that a PSC waveform is only triggered at a presynaptic firing time. Specially, as shown in Figure 4, a perturbation  $\Delta u_i^{(l)}$  of  $u_i^{(l)}[t_m]$ , i.e. due to weight updates, may result in an incremental shift in the firing time  $\Delta t$ , which in turn shifts the onset of the PSC waveform corresponding to the shifted spike, leading to a perturbation  $\Delta a_i^{(l)}$  of  $a_i^{(l)}[t_k]$ . We consider this as an inter-neuron depen-

dency since the change in PSC ( $\Delta a_i^{(l)}$ ) alters the membrane potential of the postsynaptic neuron in the next layer.

We make two important points: 1) instead of performing “fictitious” smoothing of the all-or-none spiking activation, we shall capture the inter-neuron dependencies via (the incremental changes of) the presynaptic firing times, which precisely corresponds to how different neurons interact with each other in an SNN; and 2) the *inter-neuron* dependency of each neuron is PSC  $a_i^{(l)}$  at  $t_k$  on its membrane potential  $u_i^{(l)}$  at  $t_m$  happens only if the neuron fires at  $t_m$ .

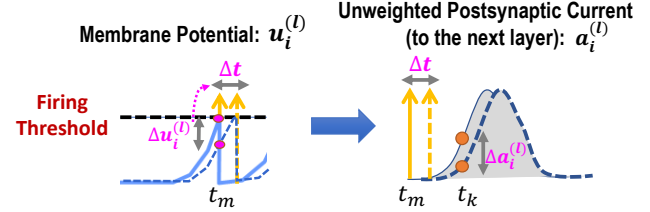


Figure 4. Inter-neuron dependencies via presynaptic firings.

In general,  $a_i^{(l)}[t_k]$ ’s inter-neuron dependencies on *all* preceding presynaptic firing times shall be considered. Figure 5 shows the situation where  $a_i^{(l)}[t_k]$  depends on two presynaptic firing times  $t_m$  and  $t_p$ . Conversely, the inter-neuron dependencies  $\phi_i^{<1>}(t_k, t_m) = 0$  if  $t_k < t_m$  or there is no spike at  $t_m$ .

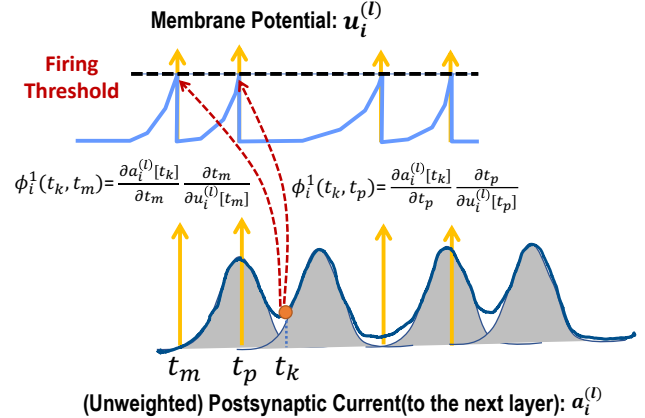


Figure 5. PSC dependencies on two preceding presynaptic firings.

Assuming that the presynaptic neuron  $i$  spikes at  $t_m$ , we derive the inter-neuron dependencies according to

$$\phi_i^{<1>}(t_k, t_m) = \frac{\partial a_i^{(l)}[t_k]}{\partial t_m} \frac{\partial t_m}{\partial u_i^{(l)}[t_m]}, \quad (15)$$

where, importantly, the chain rule is applied through the presynaptic firing time  $t_m$ .

From (2), the first part of (15) can be calculated as

$$\frac{\partial a_i^{(l)}[t_k]}{\partial t_m} = \frac{\partial(\epsilon * s_j[t_m])[t_k]}{\partial t_m}. \quad (16)$$

We adopt the approach in (Bohte et al., 2002; Ghosh-Dastidar & Adeli, 2009) to compute the second part of (15) as

$$\frac{\partial t_m}{\partial u_i^{(l)}[t_m]} = \frac{-1}{\frac{\partial u_i^{(l)}[t_m]}{\partial t_m}}, \quad (17)$$

where  $\frac{\partial u_i^{(l)}[t_m]}{\partial t_m}$  is obtained by differentiating (3).

### 3.3.4. INTRA-NEURON BACKPROPAGATION

Now we derive the intra-neuron dependency  $\phi_i^{<2>}(t_k, t_m)$  defined between two arbitrary time points  $t_k$  and  $t_m$  ( $t_m < t_k$ ), capturing the membrane potential's dependency on its history. Four different cases shall be considered due to the complications created by the relative temporal ordering of  $t_k$  and  $t_m$  and related firing activities of the same neuron, as shown in Figure 6.

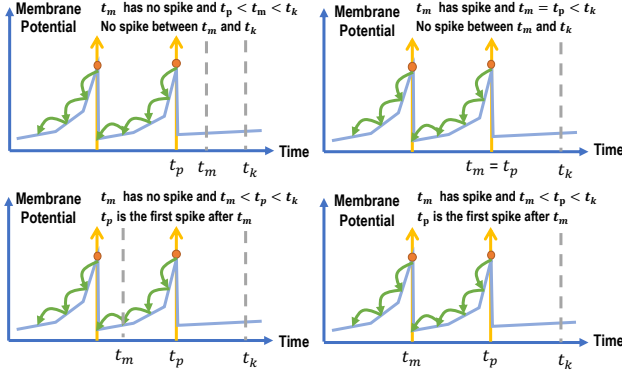


Figure 6. Intra-neuron dependencies.

**Case 1** (top left of Figure 6): there's no spike at  $t_m$  nor between  $t_m$  and  $t_k$ . In other words, the firing time  $t_p$  of the latest firing prior to  $t_k$  is before  $t_m$ :  $t_p < t_m < t_k$ . The PSC  $a_i^{(l)}$  at  $t_k$  doesn't rely on the membrane potential  $u_i^{(l)}$  at  $t_m$ , implying that neither the inter-neuron dependency nor intra-neuron dependency is nonzero:  $\phi_i^{<1>}(t_k, t_m) = \phi_i^{<2>}(t_k, t_m) = \phi_i(t_k, t_m) = 0$ .

**Case 2** (top right of Figure 6): There's a spike at  $t_m$  but no other spike between  $t_m$  and  $t_k$ , hence  $t_p = t_m$ . The membrane potential  $u_i^{(l)}[t_m]$  only affects  $a_i^{(l)}[t_k]$  through the spike at  $t_m$ , which is defined to be an inter-neuron dependency and  $\phi_i^{<1>}(t_k, t_m)$  can be obtained from (15). No additional intra-neuron dependency need to be considered, i.e.,  $\phi_i^{<2>}(t_k, t_m) = 0$  and  $\phi_i(t_k, t_m) = \phi_i^{<1>}(t_k, t_m)$ .

**Case 3** (bottom left of Figure 6): There's no spike at  $t_m$  but there is at least one spike between  $t_m$  and  $t_k$ . Denote the firing time of the spike immediately after  $t_m$  by  $t_p$ , i.e.,  $t_m < t_p < t_k$ . Since there is no spike at  $t_m$ ,  $\phi_i^{<1>}(t_k, t_m) = 0$ . Furthermore, according to (3), the membrane potential depends on its value at a previous time:  $u_i^{(l)}[t_m]$  affects  $u_i^{(l)}[t_p]$ . Therefore, according to (3), the intra-neuron dependency  $\phi_i^{<2>}(t_k, t_m)$  is

$$\begin{aligned} \phi_i^{<2>}(t_k, t_m) &= \frac{\partial a_i^{(l)}[t_k]}{\partial u_i^{(l)}[t_p]} \frac{\partial u_i^{(l)}[t_p]}{\partial u_i^{(l)}[t_m]} \\ &= \phi_i(t_k, t_p) \frac{\partial u_i^{(l)}[t_p]}{\partial u_i^{(l)}[t_m]} = \phi_i(t_k, t_p) \theta_\tau^{(t_p - t_m)}. \end{aligned} \quad (18)$$

**Case 4** (bottom right of Figure 6): There's a spike at  $t_m$  and  $t_m < t_p$  where  $t_p$  is the closest spike time after  $t_m$ . In this case, membrane potential at  $t_m$  not only generates a PSC due to the firing of the neuron, but also affects the membrane potential at the next spike time  $t_p$  resulted from the firing-and-resetting mechanism of the neuron model as described in (3). The PSC  $a_i^{(l)}[t_k]$  has an inter-neuron dependency on membrane potential  $u_i^{(l)}[t_p]$  while  $u_i^{(l)}[t_p]$  is further affected by its immediately preceding firing time  $t_m$  due to the reset. Therefore, the intra-neuron dependency  $\phi_i^{<2>}(t_k, t_m)$  should take this indirect effect on  $u_i^{(l)}[t_p]$  into consideration

$$\begin{aligned} \phi_i^{<2>}(t_k, t_m) &= \frac{\partial a_i^{(l)}[t_k]}{\partial u_i^{(l)}[t_p]} \frac{\partial u_i^{(l)}[t_p]}{\partial t_m} \frac{\partial t_m}{\partial u_i^{(l)}[t_m]} \\ &= \phi_i(t_k, t_p) \frac{\partial(\nu * s_i[t_m])[t_p]}{\partial t_m} \frac{\partial t_m}{\partial u_i^{(l)}[t_m]}, \end{aligned} \quad (19)$$

where  $\nu(\cdot)$  is the reset kernel.  $\frac{\partial t_m}{\partial u_i^{(l)}[t_m]}$  is evaluated by (17).

For  $\phi_i(t_k, t_p)$  in Case 3 and 4, since  $t_p$  is a firing time and it is after  $t_m$ , at this processing step,  $\phi_i(t_k, t_p)$  would have been already computed following either Case 2 or 4.

By considering these four cases, TSSL-BP can precisely handle the dependencies of the PSC  $a_i^{(l)}$  on its membrane potential  $u_i^{(l)}$  by  $\phi_i(t_k, t_m) = \frac{\partial a_i^{(l)}[t_k]}{\partial u_i^{(l)}[t_m]} = \phi_i^{<1>}(t_k, t_m) + \phi_i^{<2>}(t_k, t_m)$ .

To sum it up, there are two key distinctions that set our approach apart from the aforementioned activation smoothing. First, the inter-neuron dependencies only occur at pre-synaptic firing times as opposed to all prior time points, latter of which is the case when the activation smoothing is jointly applied with BPTT. The handling adopted in TSSL-BP is a manifestation of all-or-none firing characteristics of spiking neurons. Second, as illustrated in Figure 4, the key step in backpropagation is the consideration of the incremental change of spiking times, which is not considered in all recent SNNs BP works.

### 3.4. Performance Enhancements

We introduce several other techniques to achieve ultra-low latency while ensuring prediction accuracy.

#### 3.4.1. REAL-VALUED INPUT ENCODING

For non-spiking datasets such as static images, the most common preprocessing is to use rate coding to convert static real-valued inputs to spiking inputs. However, this requires many time steps for coding the inputs to guarantee good performance. For static images, we directly convert the raw pixel densities into real-valued spike current inputs within a short time window (Wu et al., 2019).

#### 3.4.2. INPUT-AND-OUTPUT WEIGHTED (IOW) SPIKING NEURON MODEL

The amount of information that can be coded by a standard binary spike train is limited by its length (number of time steps). As we strive for ultra-low latency computation over a very small number of steps, e.g. five, we adopt a new weighted spike train representation in which each spike has a multi-bit weight value to increase the coding capacity. As such, each spiking neuron would receive and generate spike trains in the weighted form. As shown in Figure 7, since the received input spikes may have a weight value greater than one, the membrane potential of the neuron may rise high above the firing threshold voltage within a single time step. In this case, outputting spike trains in the standard binary form can lead to loss of input formation. We adopt a new IOW spiking model which can process multi-bit input spikes and generate multi-bit output spikes according to several levels of firing threshold. The weight of each output spike is determined by the highest level of firing threshold the membrane potential reaches to. As we show experimentally, use of the IOW neurons leads to improved performance. On the other hand, we use 2-bit weight values for the IOW model to minimize the additional overhead. The implementation of the IOW model in hardware only requires simple logic modification of the standard LIF model on digital hardware. Our implementation on field-programmable gate arrays (FPGAs) shows that the LIF model can be converted to the IOW model with extremely low hardware and energy overheads.

#### 3.4.3. HANDLING OF PRACTICAL ISSUES

Two practical circumstances need to be taken into consideration as for other spike-time based BP methods like Spike-Prop (Bohte et al., 2002; Booij & Nguyen, 2005). First, when a spike is produced by the membrane potential  $u[t]$  that barely reaches the threshold, the derivative of  $u[t]$  w.r.t time is very small. Numerically, this can make (17) large and result in an undesirable large weight update. To mitigate, we set a lower bound for this derivative. Second, absence of firing activities in spiking neurons due to low initial weight

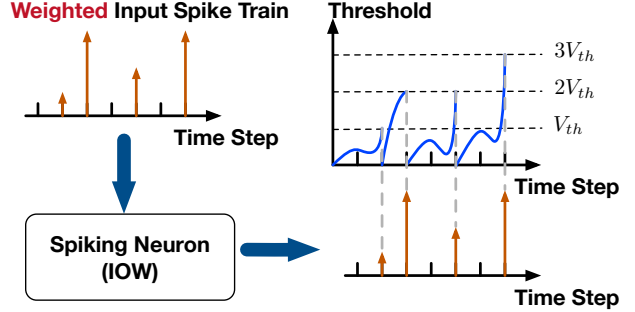


Figure 7. Input-and-Output Weighted Spiking Neuron Model

values block backpropagation through these neurons. We use a warm-up mechanism to bring up the firing activity of the network before applying the BP method.

## 4. Experiments and Results

We test the proposed TSSL-BP method on three image datasets MNIST (LeCun et al., 1998), FashionMNIST (Xiao et al., 2017) and CIFAR10 (Krizhevsky et al., 2014) with various sizes of SNNs. We compare TSSL-BP with several previously reported state-of-the-art results with the same or similar network sizes including different SNNs BP methods, converted SNNs and traditional ANNs.

### 4.1. Experimental Settings

All reported experiments below are conducted on an NVIDIA Titan XP GPU. The implementation of TSSL-BP is on the Pytorch framework (Paszke et al., 2019). The experimented SNNs are based on the LIF model described in (3). The simulation step size is set to 1 ms. Only 5 time steps are used to demonstrate low-latency spiking neural computation. The desired output spike trains (labels) for different classes are manually selected without much optimization effort. Table 1 lists the typical constant values adopted in our experiments. We use 2-bit weight values for the IOW model. No axon and synaptic delay or refractory period is used nor are normalization, regularization and dropout while incorporating these enhancements may further improve the TSSL-BP’s performance. Adam (Kingma & Ba, 2014) is adopted as the optimizer. The network models we train or compare with are either fully connected feedforward networks or convolutional neural networks (CNNs). The mean and standard deviation (stddev) of the accuracy reported below is obtained by repeating the experiments five times.

### 4.2. Datasets

The MNIST digit dataset consists of 60,000 samples for training and 10,000 for testing, each of which is a  $28 \times 28$  grayscale image. Each pixel value of an MNIST image is

Table 1. Parameters settings.

Parameter	Value
Time Constant of Membrane Voltage $\tau_m$	8 ms
Time Constant of Synapse $\tau_s$	2 ms
Threshold $V_{th}$	1 mV
Learning Rate $\eta$	0.001
Batch Size	10

converted into a real-valued input current. Each input sample is normalized to the same mean and standard deviation. No data augmentation is applied in our experiments.

The Fashion-MNIST dataset contains  $28 \times 28$  grey-scale images of clothing items, meant to serve as a much more difficult drop-in replacement for the MNIST dataset. The preprocessing steps are the same as MNIST.

The CIFAR-10 dataset contains 60,000  $32 \times 32$  color images in 10 different types of objects. There are 50,000 training images and 10,000 testing images. Similar to what are commonly adopted for preprocessing, the dataset is normalized, and random cropping and horizontal flipping are applied for data augmentation.

### 4.3. Experimental Results

#### 4.3.1. MNIST

On MNIST (LeCun et al., 1998), we compare several spiking CNNs, each of which consists of two convolutional layers, two pooling layers, and one dense layer. Table 2 compares the test accuracies of the spiking CNNs trained by the TSSL-BP method with ones trained by other algorithms. The proposed TSSL-BP delivers up to 99.53% accuracy on MNIST and outperforms all other methods except for the BP method ST-RSBP of (Zhang & Li, 2019) whose accuracy is slightly higher by 0.09%. However, compared to ST-RSBP, TSSL-BP can train high-performance SNNs with only 5 time steps, achieving  $80\times$  reduction of step count (latency). The accuracy of (Zhang & Li, 2019) drops blow that of TSSL-BP noticeably under short time windows.

#### 4.3.2. FASHIONMNIST

We compare several trained fully-connected feedforward SNNs and spiking CNNs on FashionMNIST (Xiao et al., 2017), a more challenging dataset than MNIST. In Table 3, we compare the proposed TSSL-BP with other approaches on the same feedforward network architecture of two hidden layers with each having 400 neurons. TSSL-BP achieves 90.19% test accuracy, outperforming the ST-RSBP method of (Zhang & Li, 2019), which is the best previously reported algorithm for SNNs. Moreover, TSSL-BP delivers the best test accuracy with much fewer time steps and training epochs. Table 4 compares CNNs with the same net-

work architecture. TSSL-BP noticeably outperforms the non-spiking ANN trained by a standard BP method.

Table 3. Performances of Feedforward SNNs on FashionMNIST.

Methods	Time steps	Epochs	Accuracy
ANN <sup>a</sup>		100	89.01%
HM2BP <sup>a</sup>	400	100	88.99%
ST-RSBP <sup>a</sup>	400	100	90.13%
This work (LIF neurons)	5	50	89.52%
This work (IOW neurons)	5	50	<b>90.19%</b>

<sup>a</sup> (Zhang & Li, 2019).

The network has two hidden layers with 400 neurons per layer.

Table 4. Performances of CNNs on FashionMNIST.

Methods	Time steps	Epochs	Accuracy
ANN (Xiao et al., 2017)		100	91.60%
This work (LIF neurons)	5	50	91.81%
This work (IOW neurons)	5	50	<b>92.45%</b>

The network structure is 32C5 - P2 - 64C5 - P2 - 1024: two convolutional layers, two pooling layers, and one dense layer.

Table 5. Performances of CNNs on CIFAR10.

Methods	Time steps	Epochs	Accuracy
ANN <sup>a</sup>			83.72%
Converted SNN <sup>a</sup>			83.52%
STBP (Wu et al., 2019)	8	150	85.24%
This work (IOW Neurons)	5	50	<b>87.50%</b>

<sup>a</sup> (Hunsberger & Eliasmith, 2016)

The network structure is 96C3 - 256C3 - P2 - 384C3 - P2 - 384C3 - 256C3 - 1024 - 1024: five convolutional layers, two pooling layers, and two dense layer.

#### 4.3.3. CIFAR10

Furthermore, we apply the proposed method on the more challenging dataset of CIFAR10 (Krizhevsky et al., 2014). Our TSSL-BP method achieves 87.50% accuracy with a mean of 86.78% and a standard deviation of 0.57% under five trials. As shown in Table 5, TSSL-BP delivers the best result among a previously reported ANN, an SNN converted from a pre-trained ANN, and the spiking CNN trained by the BP method of (Wu et al., 2019). Compared to MNIST, the images in CIFAR10 vary more widely in size, position, pose, and illumination. On the other hand, the long latency of all prior SNNs BP methods makes them hard to scale to deeper networks. As such, CIFAR10 is a challenging dataset for most of the existing SNNs BP methods. To the best of our knowledge, (Wu et al., 2019) is the only prior work



Table 2. Performances of Spiking CNNs on MNIST.

Methods	Network	Time steps	Epochs	Mean	Stddev	Best
Spiking CNN (Lee et al., 2016)	20C5-P2-50C5-P2-200	200 – 1000	150			99.31%
STBP (Wu et al., 2018)	15C5-P2-40C5-P2-300	> 100	200			99.42%
SLAYER (Shrestha & Orchard, 2018)	12C5-p2-64C5-p2	300	100	99.36%	0.05%	99.41%
HM2BP (Jin et al., 2018)	15C5-P2-40C5-P2-300	400	100	99.42%	0.11%	99.49%
ST-RSBP (Zhang & Li, 2019)	15C5-P2-40C5-P2-300	400	100	99.57%	0.04%	99.62%
This work (with LIF neurons)	15C5-P2-40C5-P2-300	5	100	99.39%	0.05%	99.46%
This work (with IOW neurons)	15C5-P2-40C5-P2-300	5	50	99.47%	0.05%	<b>99.53%</b>

20C5 represents convolution layer with 20 of the  $5 \times 5$  filters. P2 represents pooling layer with  $2 \times 2$  filters.

reporting BP training of SNNs on CIFAR10. The proposed TSSL-BP not only achieves 2.26% accuracy improvement over the work of (Wu et al., 2019) without the additional optimization techniques including neuron normalization, dropout, and population decoding employed in (Wu et al., 2019), but also utilizes fewer training epochs and time steps.

## 5. Conclusion

We have presented the novel temporal spike sequence learning via a backpropagation (TSSL-BP) method to train deep SNNs. The proposed TSSL-BP method properly computes the error gradient by capturing inter-neuron and intra-neuron spatiotemporal dependencies. Unlike all prior SNNs BP methods, our approach circumvents the non-differentiability of the spiking activation function while faithfully reflecting the all-or-none firing characteristics of spiking neurons and the underlying structure in the dependencies of neural activities in both time and space across the network.

We demonstrate the state-of-the-art performances in comparison with all prior SNN training methods over the MNIST, FashionMNSIT, and CIFAR10 datasets. Furthermore, the proposed TSSL-BP approach outperforms the conventional deep learning models with the same network structures.

The performances and efficiency achieved by the presented approach may be attributed to several facts: 1) proper handling the challenges in capturing spatiotemporal dependencies, 2) precise gradient computation from the all-or-none firing characteristics of spiking neurons, and 3) performance enhancement based on the IOW neuron model with low additional implementation overhead. As such, TSSL-BP provides a universal BP tool for learning arbitrarily specified target firing sequences with high accuracy while achieving low temporal latency. It has demonstrated improved scalability to deeper networks and encouraging results on datasets challenging to spiking network models.

## References

Akopyan, F., Sawada, J., Cassidy, A., Alvarez-Icaza, R., Arthur, J., Merolla, P., Imam, N., Nakamura, Y., Datta,

P., Nam, G.-J., et al. Truenorth: Design and tool flow of a 65 mw 1 million neuron programmable neurosynaptic chip. *IEEE Transactions on Computer-Aided Design of Integrated Circuits and Systems*, 34(10):1537–1557, 2015.

Bohte, S. M., Kok, J. N., and La Poutre, H. Error-backpropagation in temporally encoded networks of spiking neurons. *Neurocomputing*, 48(1-4):17–37, 2002.

Booij, O. and tat Nguyen, H. A gradient descent rule for spiking neurons emitting multiple spikes. *Information Processing Letters*, 95(6):552–558, 2005.

Davies, M., Srinivasa, N., Lin, T.-H., Chinya, G., Cao, Y., Choday, S. H., Dimou, G., Joshi, P., Imam, N., Jain, S., et al. Loihi: A neuromorphic manycore processor with on-chip learning. *IEEE Micro*, 38(1):82–99, 2018.

Diehl, P. U., Neil, D., Binas, J., Cook, M., Liu, S.-C., and Pfeiffer, M. Fast-classifying, high-accuracy spiking deep networks through weight and threshold balancing. In *Neural Networks (IJCNN), 2015 International Joint Conference on*, pp. 1–8. IEEE, 2015.

Esser, S. K., Appuswamy, R., Merolla, P., Arthur, J. V., and Modha, D. S. Backpropagation for energy-efficient neuromorphic computing. In *Advances in Neural Information Processing Systems*, pp. 1117–1125, 2015.

Gerstner, W. and Kistler, W. M. *Spiking neuron models: Single neurons, populations, plasticity*. Cambridge university press, 2002.

Ghosh-Dastidar, S. and Adeli, H. A new supervised learning algorithm for multiple spiking neural networks with application in epilepsy and seizure detection. *Neural networks*, 22(10):1419–1431, 2009.

Hunsberger, E. and Eliasmith, C. Training spiking deep networks for neuromorphic hardware. *arXiv preprint arXiv:1611.05141*, 2016.

Jin, Y., Zhang, W., and Li, P. Hybrid macro/micro level back-propagation for training deep spiking neural networks. In *Advances in Neural Information Processing Systems*, pp. 7005–7015, 2018.

- Kingma, D. P. and Ba, J. Adam: A method for stochastic optimization. *arXiv preprint arXiv:1412.6980*, 2014.
- Krizhevsky, A., Nair, V., and Hinton, G. The cifar-10 dataset. online: <http://www.cs.toronto.edu/kriz/cifar.html>, 2014.
- LeCun, Y., Bottou, L., Bengio, Y., and Haffner, P. Gradient-based learning applied to document recognition. *Proceedings of the IEEE*, 86(11):2278–2324, 1998.
- Lee, J. H., Delbruck, T., and Pfeiffer, M. Training deep spiking neural networks using backpropagation. *Frontiers in neuroscience*, 10:508, 2016.
- Maass, W., Natschl ger, T., and Markram, H. Real-time computing without stable states: A new framework for neural computation based on perturbations. *Neural computation*, 14(11):2531–2560, 2002.
- Paszke, A., Gross, S., Massa, F., Lerer, A., Bradbury, J., Chanan, G., Killeen, T., Lin, Z., Gimelshein, N., Antiga, L., Desmaison, A., Kopf, A., Yang, E., DeVito, Z., Raison, M., Tejani, A., Chilamkurthy, S., Steiner, B., Fang, L., Bai, J., and Chintala, S. Pytorch: An imperative style, high-performance deep learning library. In *Advances in Neural Information Processing Systems 32*, pp. 8024–8035. Curran Associates, Inc., 2019.
- Sengupta, A., Ye, Y., Wang, R., Liu, C., and Roy, K. Going deeper in spiking neural networks: Vgg and residual architectures. *Frontiers in neuroscience*, 13, 2019.
- Shrestha, S. B. and Orchard, G. Slayer: Spike layer error reassignment in time. In *Advances in Neural Information Processing Systems*, pp. 1412–1421, 2018.
- Tavanaei, A., Ghodrati, M., Kheradpisheh, S. R., Masquelier, T., and Maida, A. Deep learning in spiking neural networks. *Neural Networks*, 2018.
- Werbos, P. J. Backpropagation through time: what it does and how to do it. *Proceedings of the IEEE*, 78(10):1550–1560, 1990.
- Wu, Y., Deng, L., Li, G., Zhu, J., and Shi, L. Spatio-temporal backpropagation for training high-performance spiking neural networks. *Frontiers in neuroscience*, 2018.
- Wu, Y., Deng, L., Li, G., Zhu, J., Xie, Y., and Shi, L. Direct training for spiking neural networks: Faster, larger, better. In *Proceedings of the AAAI Conference on Artificial Intelligence*, volume 33, pp. 1311–1318, 2019.
- Xiao, H., Rasul, K., and Vollgraf, R. Fashion-mnist: a novel image dataset for benchmarking machine learning algorithms. *arXiv preprint arXiv:1708.07747*, 2017.
- Xu, Y., Zeng, X., Han, L., and Yang, J. A supervised multi-spike learning algorithm based on gradient descent for spiking neural networks. *Neural Networks*, 43:99–113, 2013.
- Zhang, W. and Li, P. Spike-train level backpropagation for training deep recurrent spiking neural networks. In *Advances in Neural Information Processing Systems*, pp. 7800–7811, 2019.